ARMA 15-536

Parametric study of smooth joint parameters on the behavior of inherently anisotropic rock under uniaxial compression condition

Duan, K. and Kwok, C.Y.

Department of Civil Engineering, The University of Hong Kong, Hong Kong

This paper was prepared for presentation at the 49th US Rock Mechanics / Geomechanics Symposium held in San Francisco, CA, USA, 28 June-1 July 2015.

ABSTRACT: Inherently anisotropic rocks are modeled with the use of two-dimensional Discrete Element Methods (DEM). In the simulated anisotropic rock sample, the rock matrix is modeled as an assembly of rigid particles and the existence of weak layers is directly represented by imposing individual smooth joint (SJ) contacts with same orientation into the rock matrix. The properties of a SJ contact include normal and shear stiffness, normal strength, cohesion, and friction angle. A systematic study is conducted to investigate the influence of these parameters on the macro behaviors of anisotropic rocks with different anisotropy angles under uniaxial compression condition. The Young's modulus is found to increase significantly with the SJ normal stiffness when the anisotropy angle is low (0^o-30^o). The USC increases with the SJ normal strength at high anisotropy angle (β>60°) while cohesion raises the UCS at medium anisotropy angle (30^o-60^o). The influence of friction angle is not significant. Understanding the influence of each parameter is of great importance for the calibration of micro parameters to represent certain type of rock. A general process for the calibration of micro parameters to reproduce the strength and deformation behaviors of different types of anisotropic rocks is proposed.

1. INTRODUTION

Anisotropy is everywhere while isotropy is rare [1]. Many rocks are characterized by a structural inherent anisotropy which is due to the existence of rock fabric elements such as bedding, layering, foliation and lamination planes [2]. Such rocks are said to be inherently anisotropic as their physical, mechanical and hydraulic properties vary with direction. Rock anisotropy affects many rock related projects, e.g., borehole stability [3], propagation of hydraulic fracturing [2], and deviation of drilling. Therefore, a complete understanding of the behaviors of anisotropic rocks under different stress conditions is extremely important.

In the past several decades, many investigators have performed compression tests on various anisotropic rocks, e.g., Niandou et al. [4] on shale, Nasseri et al.[5] on schists, Tien et al. [6] on artificial materials. In general, the variation of failure strength with the anisotropy angle is characterized by a U-shaped curve with the minimum strength obtained when the anisotropy angle (β) is around 60^o. In fact, the geometry of the curves as well as the failure modes with different anisotropy angles vary for different types of rocks [4]. Attempts have also been made aiming to investigate the effect of weak planes orientation on the behaviors of anisotropic rocks on the micro-scale through laboratory testing [7, 8]. However, it is very difficult to explore the micro-scale mechanisms from laboratory testing which leads to a lack of a thorough understanding of the underlying failure mechanisms.

Numerical tools which are able to reproduce the observed failure mechanisms are required. The discrete element method (DEM) offers unique advantage of being able to explicitly model the formation and propagation of fractures in rocks. Particle-based DEM model has been successfully applied in modeling the behavior of isotropic rocks under different stress conditions [9-11]. The anisotropic behaviors of jointed rock mass have been studied based on the smooth joint contact model [12, 13]. Most recently, the behaviors of anisotropic rock was simulated by inserting a series of continuous smooth joint contacts [14]. However, these structures are more like those of induced fractures normally encountered in jointed rock masses.

For the intact anisotropic rocks, the bedding planes at micro-scale may not be necessarily straight and continuous, as shown in Fig. 1 (a) [15]. Therefore, there is a need to develop a more realistic numerical approach to explicitly represent the weak layers in micro-scale. In this study, existence of inherently anisotropy are explicitly represented by imposing individual smooth-joint (SJ) contacts [16] into the bonded-particle model (BPM) with the same orientation. The effects of smooth joint parameters on the macroscopic properties (UCS and Young's modulus) under uniaxial compression test are systematically investigated.

2. GENESIS OF NUMERICAL MODEL

In this study, the transverse anisotropy, which has a set of parallel planes of weakness, is modeled. The generated anisotropic rock model with horizontal weak layers (β=0^o) is illustrated in Fig. 1(b). The first step is to create an isotropic model based on the bonded particle model (BPM) to represent the rock matrix [9]. To introduce horizontal anisotropy, any sub-horizontal parallel bonds (those dipping within -20^o~+20^o, for instance) are removed and replaced by horizontal smooth-joint contacts (dipping 0^o). The smooth-joint model simulates the behavior of an interface regardless of the local particle contact orientations along the interface. These individual smooth joints represent the discontinuous weak beddings in inherently anisotropic rocks as illustrated in Fig. 1(a). Rocks with different degrees of anisotropy can be modeled by including different amounts and properties of smooth joints.

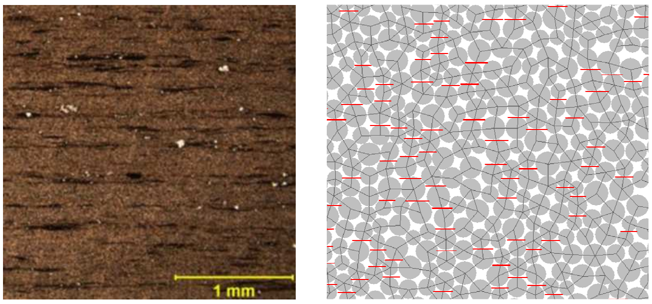

(a) (b)

Fig 1. (a) Thin-section image of Bossier Shale [15]; (b) Proposed DEM model.

The macro properties of bonded particle model for rocks are determined by the micro parameters of BPM, including the size distribution of particles, strengths of parallel bonds ($\bar{\sigma}_c$ and $\bar{\tau}_c$), stiffnesses of particles (k^n and k^s), stiffnesses of parallel bonds ($\bar{k}^n$ and $\bar{k}^s$), and friction coefficient between particles (μ_c).The recommended calibration procedure for bonded particle model can be found in [17].

Smooth joint parameters have a dominant effect on the macro behaviors of the proposed anisotropic rock model. The smooth joint parameters include normal stiffness ($\bar{k}_n$), shear stiffness ($\bar{k}_s$), bond normal strength (σ_c), and bond shear strength (τ). τ is determined as following:

$$\tau = c_b + \sigma \tan \varphi_b \tag{1}$$

where σ is the normal stress acting at the contact, c_b is the cohesion, φ_b is the friction angle. These parameters cannot be measured directly in the laboratory. Thus, a major challenge is to calibrate these micro parameters correctly to match the experimental data.

Table 1. Parameters for the isotropic model [9].

Particle properties	Value	Bond properties	Value
E_c	62 GPa	$\bar{E}_c$	62 GPa
k_n / k_s	2.5	$\bar{k}_n / \bar{k}_s$	2.5
μ	0.5	$\bar{\sigma}_c$	157±36 MPa
R_{max} / R_{min}	1.66	$\bar{\tau}_c$	157±36 MPa
R_{min}	0.2 mm	$\bar{\lambda}$	1.0
ρ	3169 kg/m^3		

In this paper, numerical models with different anisotropy angles (β=0°, 15^o, 30^o, 45^o, 60^o, 75^o, and 90^o) are generated and uniaxial compression tests are performed on these models. Micro parameters for the Lac du Bonnet Granite [9] are selected to generate the isotropic model (Table 1). The parameters of smooth joint can be inherited from parallel bond based on a series of equations [17]. The values of smooth joint parameters inherited from parallel bonds are listed in Table 2. These parameters are adopted as the control test as they give responses closest to an isotropic model.

Table 2. Micro parameters for smooth joint model inherited from parallel bond.

Normal stiffness, $\bar{k}_n$ (GPa/m)	~250000
Shear stiffness, $\bar{k}_s$ (GPa/m)	~100000
Friction coefficient, μ	0.5
Dilation angle, ψ (degree)	0
Tensile strength, σ_c (MPa)	157
Cohesion, c_b (MPa)	157
Friction angle, φ_b (degree)	0

3. PARAMETRIC STUDY

In this Section, the micro parameters of smooth joints are reduced systematically to evaluate their effects on the deformability and strength of anisotropic models. It is worth emphasizing that in this parametric study, we are not trying to reproduce the elastic response of a certain rock type and the responses are normalized by the results obtained in the control test (UCS= 204.6 MPa, E= 74.5 GPa) as a dimensionless analysis. This exercise provides a fundamental understanding of how the micro-scale properties control the macro mechanical behaviors of rocks with different degrees of anisotropy. Understanding the influence of each parameter is also of great importance for the calibration of micro parameters to represent certain type of rock

3.1. *Effect of smooth joint strength*

The effect of smooth joint strength is investigated by reducing the normal strength (σ_c) and cohesion (c_b) of smooth joint simultaneously with a factor of 1, 0.5, 0.2, 0.1 and 0.06. Other parameters are inherited from parallel bonds and kept constant.

The variations of normalized UCS and E are illustrated in Figure 2(a) and (b), respectively. The decreasing of smooth joint strength reduces the UCS and E at high anisotropy angles (β>30°). No significant effect can be found at low anisotropy angles as the weak layers are under compression at these directions and failure are mainly formed as crack of parallel bonds. Another phenomenon worth noting is that the effect of reducing smooth joint strength become stable when the factor is low enough (0.2 for UCS and 0.1 for Young's modulus).

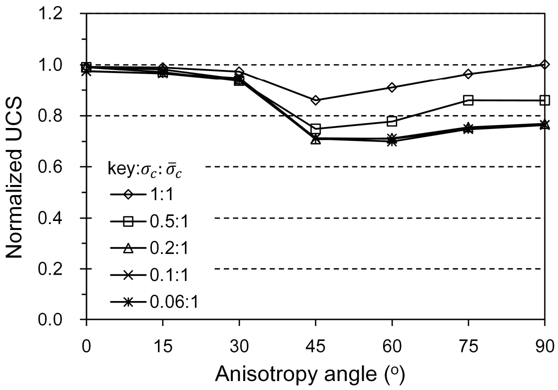

(a) Normalized UCS

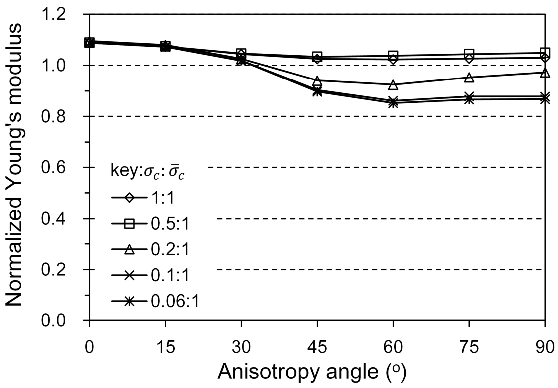

(b) Normalized Young's modulus

Fig 2. Effect of smooth joint strength.

3.2. *Effect of smooth joint stiffness*

The effect of smooth joint stiffness is investigated by reducing $\bar{k}_n$ and $\bar{k}_s$ with a factor of 1, 0.6, 0.4, 0.2, 0.1, and 0.05 while keeping them equal. The strength of smooth joint is 1/5 of parallel bond. The simulation results are presented in Figure 3. It can be concluded that the stiffness plays an important role at low anisotropy angles (β<45^o) where both the UCS and E decrease with the decreasing of smooth joint stiffness. When the smooth joint stiffness is reduced to 0.05 of parallel bond, the minimum UCS is obtained when β=0^o, which deviates from the general U-shaped curve of UCS. Therefore, this value cannot be extremely low. At high anisotropy angles (β>45^o), the effect of stiffness becomes weak. Further study is conducted in Section 3.5 to investigate the effect of normal and shear stiffness separately.

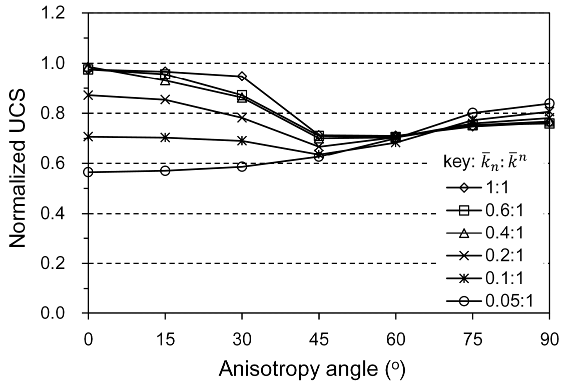

(a) Normalized UCS

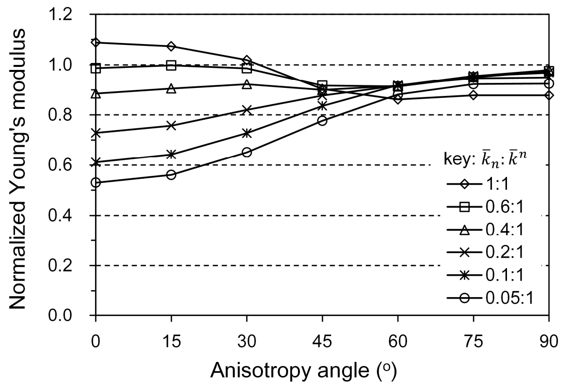

(b) Normalized Young's modulus

Fig. 3. Effect of smooth joint stiffness.

3.3. *Effect of ratio between normal strength and cohesion*

As demonstrated in Eq. (1), the shear strength of smooth joint is determined by the combination of cohesion (c_b), normal strength (σ_c), friction angle (φ_b), and the compression stress acting on the smooth joint. The effect of ratio between normal strength and cohesion is studied in this section and the effect of the friction angle is discussed in the Section 3.4.

In Fig. 4, the cohesion of smooth joint (c_b) is kept constant as 1/5 of parallel bond and the normal strength (σ_c) is varied by a factor of 0.5, 1, 2 and 4. As can be observed in Figure 4(a) and (b), the UCS at high anisotropy angle (75^o-90^o) increases with the increase of normal strength. At low and medium anisotropy angles (β<60^o), this effect becomes negligible.

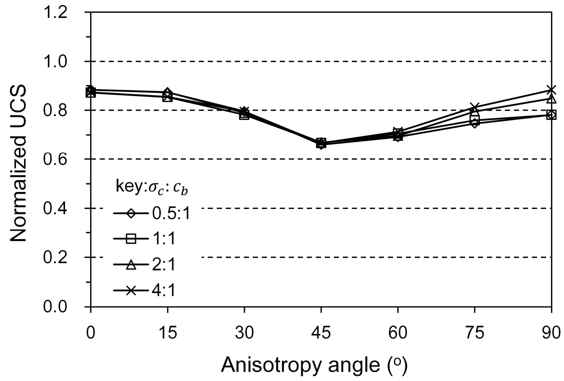

(a) Normalized UCS

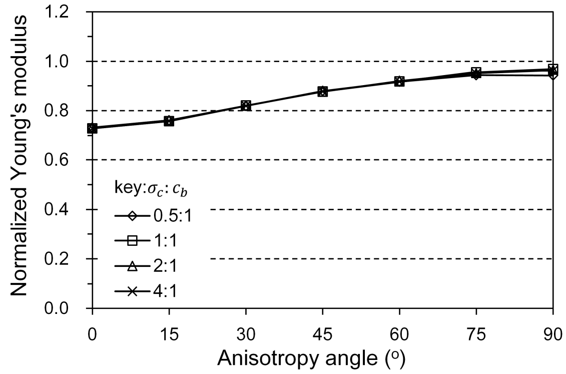

(b) Normalized Young's modulus

Fig. 4. Effect of ratio between normal strength and cohesion of smooth joint contact.

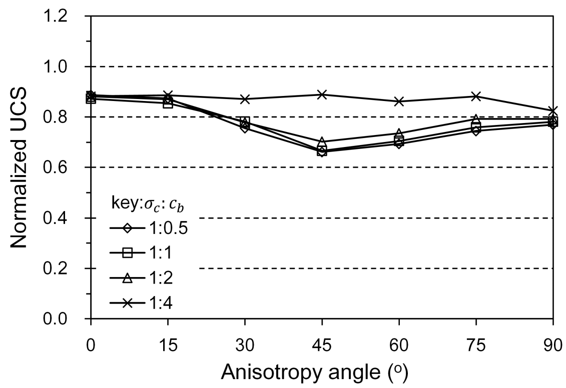

(a) Normalized UCS

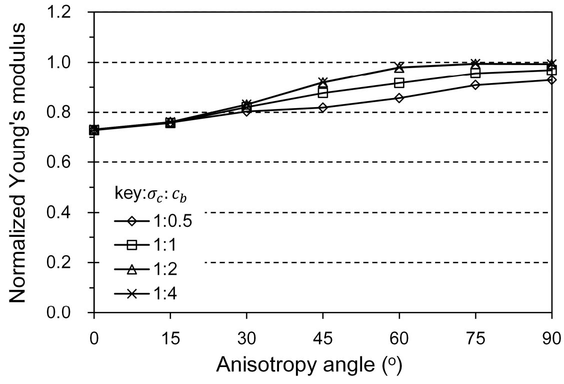

(b) Normalized Young's modulus

Fig.5. Effect of ratio between normal strength and cohesion of smooth joint contact

In Fig 5, the effect of cohesion is investigated by increasing the cohesion of smooth joint while keeping the normal strength constant as 1/5 of parallel bond. As expected, increasing the cohesion of smooth joint significantly increase the UCS at intermediate anisotropy angles (30o-75o). Meanwhile, the Young's modulus when β>30o increase. As the shear strength of smooth joint increase, shear failure of smooth joint become hard to develop at this direction. When the cohesion of smooth joint reaches 4 times of normal strength, the UCS curve turns out to be flatten which means that the numerical model becomes almost isotropic.

3.4. *Effect of friction angle*

Different friction angles (φ=0^o, 10^o, 20^o, 30^o, and 40^o) are assigned to the smooth joint while other parameters are kept constant. The simulation results are illustrated in Fig. 6. As expected, increasing the friction angle affects the behaviors at intermediate anisotropy angles (30^o-60^o). Both the UCS and the Young's modulus increase with the increasing of friction angle at these directions. These results are consistent with that from Section 3.3 which is due to the increasing of smooth joint shear strength.

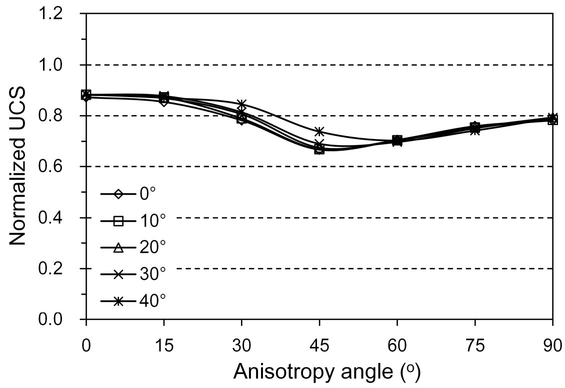

(a) Normalized UCS

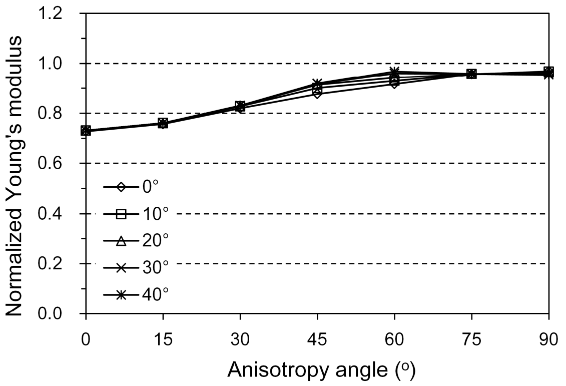

(b) Normalized Young's modulus

Fig. 6 Effect of friction angle.

3.5. Effect of ratio between normal and shear stiffness

The effect of smooth joint stiffness is further examined by looking at the effect of either normal or shear stiffness separately. Two scenarios are considered: keep one of them constant and vary the other gradually. Other parameters stay constant for all these cases. The simulation results are presented in Fig. 7 and Fig. 8, respectively.

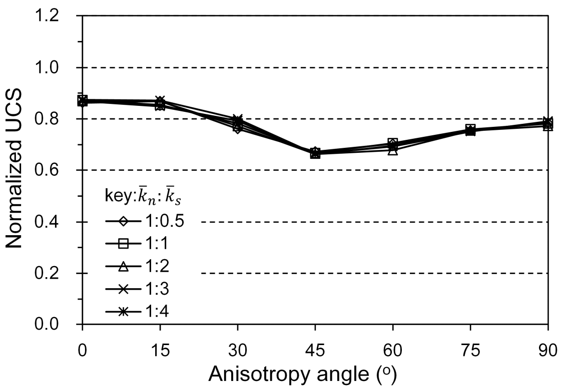

(a) Normalized UCS

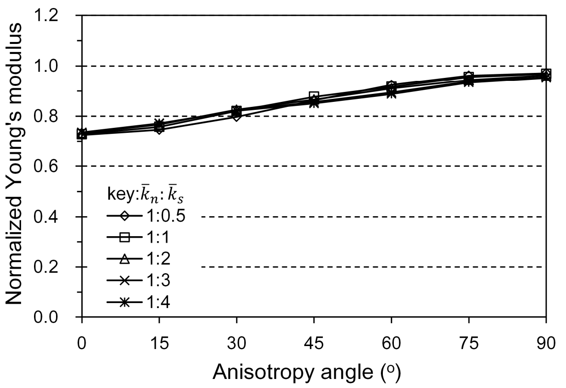

(b) Normalized Young's modulus

Fig. 7 Effect of ratio between normal and shear stiffness of smooth joint (normal stiffness is constant).

In Fig. 7, the normal stiffness ($\bar{k}_n$) is constant (1/5 of parallel bond) and shear stiffness ($\bar{k}_s$) is varied by different ratios. The simulated results reveal that changing the shear stiffness does not affect the macroscopic properties much.

Different results are obtained when change the normal stiffness of smooth joint, as shown in Fig. 8. Both the UCS and Young's modulus increase with the increase of smooth joint normal stiffness. Therefore, the normal stiffness of smooth joint plays a dominant role on the macroscopic response at low anisotropy angles.

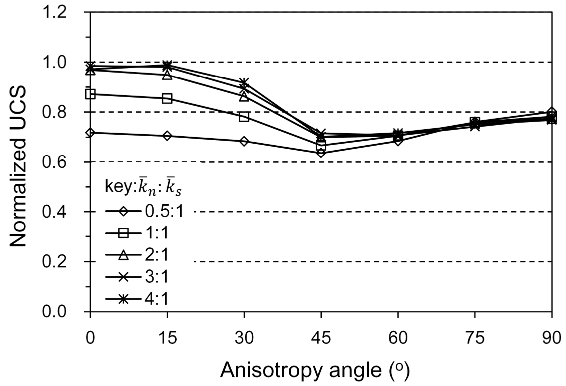

(a) Normalized UCS

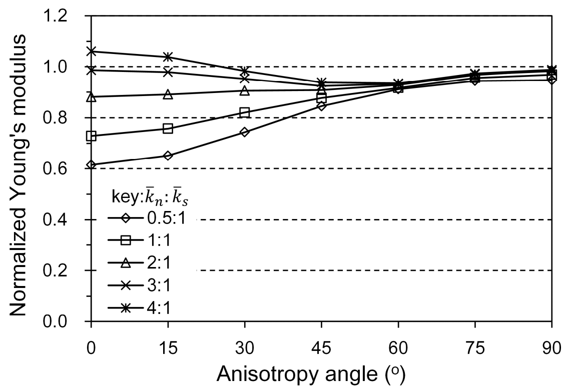

(b) Normalized Young's modulus

Fig. 8 Effect of ratio between normal and shear stiffness of smooth joint contact (shear stiffness is constant).

3.6. Effect of angle range

The angle range determines the amount of parallel bonds being replaced by smooth joint contacts, which ultimately affects the degree of anisotropy of the numerical model. In this section, samples with different angle ranges (±10^o, ±20^o, ±30^o, ±40^o, and ±50^o) are generated and tested. As expected, the degree of anisotropy increases with the increasing of angle range. As illustrated in Fig. 9, the anisotropy ratio of UCS (UCS_{max}/UCS_{min}) increases from 1.23 to 2.86 when the angle range increases from ±10^o to ±50^o. At the same time, the normalized Young's modulus when β=0^o decreases from 0.82 to 0.6. Therefore, this parameter can be tuned to represent rocks with different degrees of anisotropy.

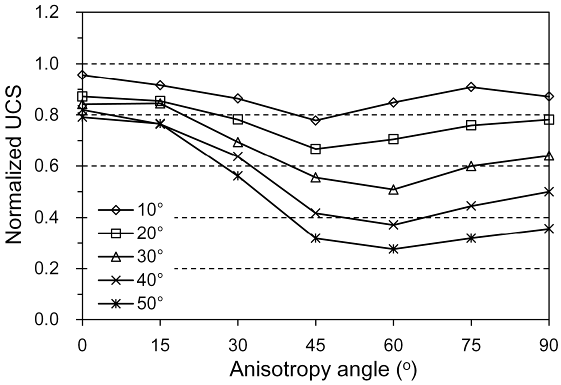

(a) Normalized UCS

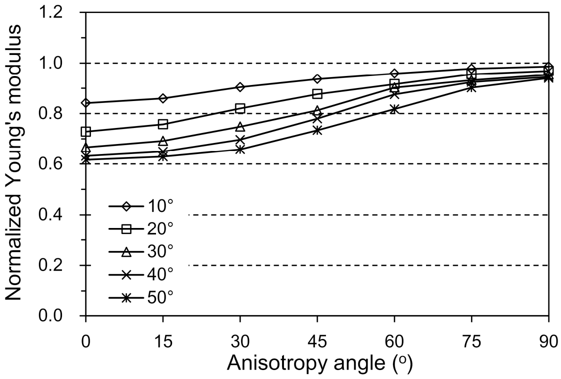

(b) Normalized Young's modulus

Fig. 9. Effect of angle range.

4. CALIBRATION

Based on the parametric study results discussed in Section 3, the following procedures are proposed for the calibration of micro parameters for anisotropic rocks:

(i) The angle range of parallel bonds being replaced is first selected. A reasonable value to start with is $\pm 10^{o}$.

(ii) The stiffness of parallel bond can be calibrated to match the Young's modulus when $\beta=90^{o}$ as the effect of smooth joint stiffness is minimum at this direction.

(iii) The stiffness of smooth joint is calibrated to match the Young's modulus when $\beta=0^{o}$. The values matched in step (ii) may also be decreased. Thus, iterations between step (ii) and (iii) might be required to match the entire curve of Young's modulus.

(iv) The strength of parallel bond can be calibrated to match the UCS when $\beta=0°$. This direction is selected as weak layers are under compression and the strength of smooth joint does not affect the UCS much.

(v) The strength of smooth joint can be calibrated to match the UCS when $\beta=90°$.

If the anisotropy ratio cannot be reproduced, it is necessary to increase the angle range and the procedures between (i)-(v) should be repeated.

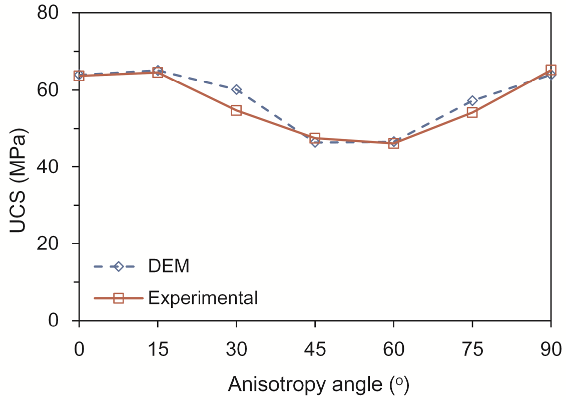

(a) Variation of UCS

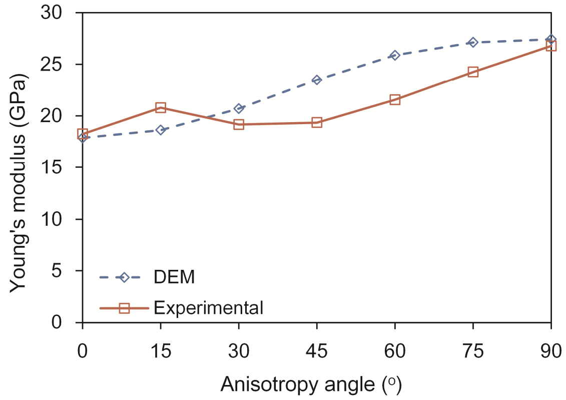

(b) Variation of Young's modulus

Fig. 10. Comparison of simulated and experimental results from an Outcrop Shale [18].

Table 3. Micro parameters calibrated for an Outcrop Shale [18].

Particle	E_c (GPa)	23
Parallel bond	$\overline{E}_c$ (GPa)	23
	$\overline{\sigma}_c$ (MPa)	60±13.5
	$\overline{\tau}_c$ (MPa)	60±13.5
Smooth-joint	Angle rang	±30°
	Normal stiffness, $\overline{k}_n$ (GPa/m)	17,500
	Shear stiffness, $\overline{k}_s$ (GPa/m)	17,500
	Tensile strength, σ_c	30
	Cohesion, c_b	22
	Friction angel (°)	0

Following the guidelines described above, the numerical model is calibrated to represent an Outcrop Shale [18]. The comparison between experimental and simulated results in terms of UCS and Young's modulus is presented in Figure 10 (a) and (b), respectively. The calibrated micro parameters are listed in Table 3. Good agreement can be found between the simulated and experimental results.

5. CONCLUSIONS

This study proposes a numerical approach to represent the micro structure of anisotropic rocks by inserting smooth joint models into bonded particle model. Based on this numerical approach, parametric studies are conducted to evaluate the effect of weak layer properties on the macroscopic behaviors of anisotropic rock under uniaxial compression test.

The simulation results reveal that the Young's modulus significantly increases with the smooth joint normal stiffness when the anisotropy angle is low (0^o-30^o). The normal stiffness of smooth joint plays a dominant role while the effect of shear stiffness is found to be negligible. USC increases with the smooth joint normal strength at high anisotropy angle (β>60°). The cohesion and friction angle of smooth joint controls the shear strength of smooth joint which ultimately determines the failure strength and stiffness at medium anisotropy angles (30^o-60^o). The angle range of parallel bonds being replaced affects the anisotropy ratio which can be tuned to represent rocks with different degree of anisotropy.

Understanding the effect of each parameter is essential for the calibration of numerical model. A detailed guideline for the calibration of micro parameters is provided. The numerical model can reproduce both the strength and stiffness of anisotropic rock quantitatively. Moreover, parametric studied provide some innovative understanding about the microscopic mechanism of different anisotropic rocks with different loading directions.

ACKNOWLEDGEMENT

The research was funded by the Natural Science Fund of China (NSFC) (Grant No. 51428902).

REFERENCES

1. Barton, N. and E. Quadros. 2014. Anisotropy is Everywhere, to See, to Measure, and to Model. *Rock Mechanics and Rock Engineering*: p. 1-17.

2. Amadei, B. 1996. Importance of anisotropy when estimating and measuring in situ stresses in rock. *International Journal of Rock Mechanics and Mining Sciences & Geomechanics Abstracts*, **33**(3): p. 293-325.

3. Zhang, J. 2013. Borehole stability analysis accounting for anisotropies in drilling to weak bedding planes. *International Journal of Rock Mechanics and Mining Sciences*, **60**(0): p. 160-170.

4. Niandou, H., et al. 1997. Laboratory investigation of the mechanical behaviour of Tournemire shale. *International Journal of Rock Mechanics and Mining Sciences*, **34**(1): p. 3-16.

5. Nasseri, M., K. Rao, and T. Ramamurthy. 2003. Anisotropic strength and deformational behavior of Himalayan schists. *International Journal of Rock Mechanics and Mining Sciences*, **40**(1): p. 3-23.

6. Tien, Y.M., M.C. Kuo, and C.H. Juang. 2006. An experimental investigation of the failure mechanism of simulated transversely isotropic rocks. *International journal of rock mechanics and mining sciences*, **43**(8): p. 1163-1181.

7. Brown, E.T., S.J. Green, and K.P. Sinha. 1981. The influence of rock anisotropy on hole deviation in rotary drilling— A review. *International Journal of Rock Mechanics and Mining Sciences & Geomechanics Abstracts*, **18**(5): p. 387-401.

8. Wu, X.Y., P. Baud, and T.-f. Wong. 2000. Micromechanics of compressive failure and spatial evolution of anisotropic damage in Darley Dale sandstone. *International Journal of Rock Mechanics and Mining Sciences*, **37**(1–2): p. 143-160.

9. Potyondy, D.O. and P.A. Cundall. 2004. A bonded-particle model for rock. *International Journal of Rock Mechanics and Mining Sciences*, **41**(8): p. 1329-1364.

10. Park, J. and J.J. Song. 2009. Numerical simulation of a direct shear test on a rock joint using a bonded-particle model. *International Journal of Rock Mechanics and Mining Sciences*, **46**(8): p. 1315-1328.

11. Duan, K., C.Y. Kwok, and L.G. Tham. 2015. Micromechanical analysis of the failure process of brittle rock. *International Journal for Numerical and Analytical Methods in Geomechanics*, **39**(6): p. 618-634.

12. Chiu, C.-C., et al. 2013. Modeling the anisotropic behavior of jointed rock mass using a modified smooth-joint model. *International Journal of Rock Mechanics and Mining Sciences*, **62**(0): p. 14-22.

13. Bahaaddini, M., G. Sharrock, and B. Hebblewhite. 2013. Numerical investigation of the effect of joint geometrical parameters on the mechanical properties of a non-persistent jointed rock mass under uniaxial compression. *Computers and Geotechnics*, **49**: p. 206-225.

14. Park, B. and K.-B. Min. *Discrete Element Modeling of Transversely Isotropic Rock*. in *47th US Rock Mechanics/Geomechanics Symposium*. 2013. American Rock Mechanics Association.

15. Ambrose, J., R.W. Zimmerman, and R. Suarez-Rivera, 2014, Failure of shales under triaxial compressive stress, in *the 48th US Rock Mechanics/Geomechanics Symposium*: Minneapolis, MN, USA.

16. Ivars, D.M., et al. 2011. The synthetic rock mass approach for jointed rock mass modelling. *International Journal of Rock Mechanics and Mining Sciences*, **48**(2): p. 219-244.

17. Itasca, 2010, PFC2D Particle Flow Code in 2 Dimensions: Minneapolis.

18. Fjær, E. and O.-M. Nes. 2014. The Impact of Heterogeneity on the Anisotropic Strength of an Outcrop Shale. *Rock Mechanics and Rock Engineering*, **47**(5): p. 1603-1611.